Annu. Rev. Mater. Res. 2002. 32:347–75
doi: 10.1146/annurev.matsci.32.112601.134925

MECHANICAL AND ELECTRICAL PROPERTIES OF NANOTUBES

J. Bernholc,[1] D. Brenner,[2] M. Buongiorno Nardelli,[1] V. Meunier,[1] and C. Roland

[1]Department of Physics and [2]Department of Materials Science and Engineering, North Carolina State University, Raleigh, North Carolina 27695; e-mail: bernholc@ncsu.edu; brenner@eos.ncsu.edu; mbnardelli@ncsu.edu; roland@gatubela.physics.ncsu.edu

Key Words composites, deformation, STM images, STS spectra

■ **Abstract** We review the recent progress in our understanding of the mechanical and electrical properties of carbon nanotubes, emphasizing the theoretical aspects. Nanotubes are the strongest materials known, but the ultimate limits of their strength have yet to be reached experimentally. Modeling of nanotube-reinforced composites indicates that the addition of small numbers of nanotubes may lead to a dramatic increase in the modulus, with only minimal crosslinking. Deformations in nanotube structures lead to novel structural transformations, some of which have clear electrical signatures that can be utilized in nanoscale sensors and devices. Chemical reactivity of nanotube walls is facilitated by strain, which can be used in processing and functionalization. Scanning tunneling microscopy and spectroscopy have provided a wealth of information about the structure and electronic properties of nanotubes, especially when coupled with appropriate theoretical models. Nanotubes are exceptional ballistic conductors, which can be used in a variety of nanodevices that can operate at room temperature. The quantum transport through nanotube structures is reviewed at some depth, and the critical roles played by band structure, one-dimensional confinement, and coupling to nanoscale contacts are emphasized. Because disorder or point defect–induced scattering is effectively averaged over the circumference of the nanotube, electrons can propagate ballistically over hundreds of nanometers. However, severe deformations or highly resistive contacts isolate nanotube segments and lead to the formation of quantum dots, which exhibit Coulomb blockade effects, even at room temperature. Metal-nanotube and nanotube-nanotube contacts range from highly transmissive to very resistive, depending on the symmetry of two structures, the charge transfer, and the detailed rehybridization of the wave functions. The progress in terms of nanotube applications has been extraordinarily rapid, as evidenced by the development of several nanotube-based prototypical devices, including memory and logic circuits, chemical sensors, electron emitters and electromechanical actuators.

INTRODUCTION

Carbon is unique among the elements in its ability to assume a wide variety of different structures and forms. It is now a little more than ten years since nanotubes were discovered (1), creating a plethora of opportunities in science and technology for novel materials and devices. Carbon nanotubes are hollow cylinders consisting of single or multiple sheets of graphite (graphene) wrapped into a cylinder, as illustrated in Figure 1. They have extraordinary structural, mechanical, and electrical properties that derive from the special properties of carbon bonds, their unique quasi-one-dimensional nature, and their cylindrical symmetry. For instance, the graphitic network upon which the nanotube structure is based is well known for its strength and elasticity, thereby providing unmatched mechanical strength. Nanotubes can also be metallic or semiconducting, depending on their helicity indices (see Figure 1), which opens up the interesting prospects of nanotube-based junctions and devices. Originally, nanotubes were synthesized in minute quantities only, and very few experimental techniques were available for their study. Their discovery, however, has stimulated much theoretical work. These investigations have benefited significantly from the substantial progress achieved in the past two to three decades in the development of theoretical methods, some of which now have a truly predictive power. Astonishing properties have been predicted, stimulating further experiments and better growth methods. The progress has been rapid, with hundreds of nanotube-related papers being published every

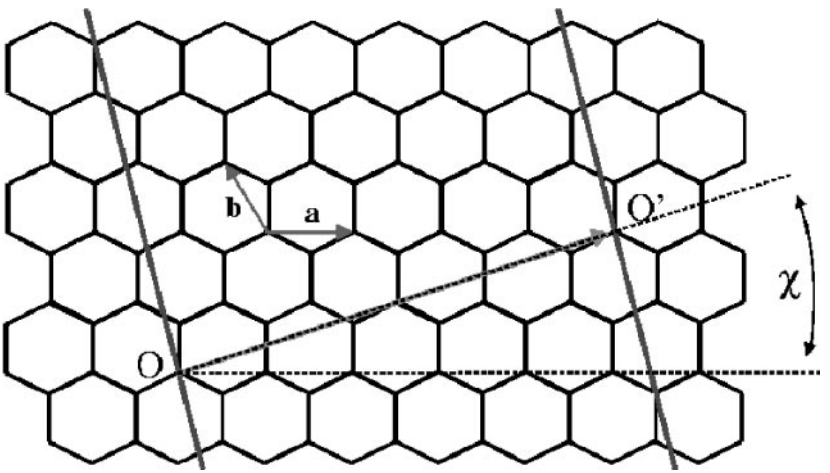

Figure 1 Nanotube structures are obtained by rolling a graphene sheet into a cylinder so that the lattice points O and O' fold onto each other. Mathematically, their structures are uniquely defined by specifying the coordinates of the smallest folding vector (n,m) in the basis of graphene lattice vectors $\vec{a}$ and $\vec{b}$. The (n,0) zigzag and (n,n) armchair tubes are mirror-symmetric; all other tubes are chiral.

year. Several recent books and articles, including extensive bibliographies, provide a comprehensive description of the early progress in the field of nanotubes (2–4).

This short review is concerned with mechanical and electrical properties of nanotubes, in which the theoretical work has played a particularly important role and offers exceptional promise for applications. Nanotubes are now well established as the strongest materials known. Their electronic properties enable ballistic transport over more than 100 nm, as well as single-electron transistors, molecular sensors, and nano-electromechanical devices.

When considering nanoscale mechanical or electrical properties, the relevant phenomena span many length and time scales, necessitating the use of a full spectrum of theoretical techniques from ab initio calculations to tight-binding and classical molecular dynamics methods. Simulations of growth (5), which fall outside the scope of this review, require lattice Monte Carlo methods in order to deal with the time scales involved. Each of these techniques is reviewed elsewhere in this volume. We thus mention only those technical aspects that are either unique or particularly important to the subject of this review.

The review is divided in two broad sections devoted to simulations of the mechanical and electrical properties. Each of these topics faces unique challenges. For example, realistic simulations of strength and mechanical failure would need to span time scales that are completely inaccessible to all but the simplest simulation techniques. The simulations of electrical properties, on the other hand, require calculation of quantum conduction through a large, open system, consisting of a device and leads that supply and remove the electrons from the active region. The computational formalism for dealing effectively with these open boundary conditions while providing a realistic description of the underlying electronic structure has been developed only very recently. For this reason, it is described in some depth below.

The simulations of mechanical properties of nanotubes have led to the surprising conclusion that a $\sim$1-nm-wide nanotube can often be treated as a narrow hollow cylinder, subject to the laws of continuum mechanics. This is true of bending, torsion, and compression, for which the various elastic moduli and continuum mechanics predict well the initial deformations. The discrete atomic structure of nanotubes manifests itself for only very large deformations or at the limits of extreme tension, where brittle or plastic behaviors were predicted and, indeed, observed. At the ultimate tension limit, the exceptional strength of carbon-carbon bonds and the perfection of the nanotube structure leads to unheard-of strengths and mechanical resilience.

The electrical properties of nanotubes are no less spectacular. Early observations of ballistic conductance (6, 7) have stimulated much experimental and theoretical work. Nanotube-based transistors and rectifiers have already been made, and many predictions and observations of nanotube junctions and structures with unique properties have been noted. The one-dimensional structure of nanotubes also leads to strong many-body effects, which manifest themselves in the occurrence of a Luttinger liquid at low temperatures. Indeed, some of the properties of nanotube devices at low temperatures follow the predicted Luttinger liquid behavior.

Mechanical deformations quickly change the electrical properties of some nanotubes, indicating their potential suitability for nanoscale strain sensors. Other nanotubes are less sensitive to strain and can form flexible nanoscale conductors.

SIMULATION OF MECHANICAL PROPERTIES

This section focuses on the mechanical properties of carbon nanotubes and discusses their elastic properties and strain-induced transformations. Only single-walled nanotubes are considered as they can be grown with many fewer defects and are thus much stronger. Because nanotubes can be viewed as "rolled-up" graphene sheets, and because graphite is exceptionally strong with respect to in-plane deformations, nanotubes possess extraordinary mechanical properties. We focus primarily on two aspects: elastic deformations, where the shape of the nanotube may change but the local atomic coordination does not; and the onset of irreversible behavior, where the atomic structure undergoes irreversible changes. In either case, nanotubes are exceptionally elastic and strong: They can reversibly bend to very high angles, and their tensile strength is unmatched by any known material. In fact, the astonishing strength of nanotubes was predicted by simulations and only later observed experimentally.

Bending and Elastic Deformations

The first simulations of elastic properties of nanotubes were stimulated by the experimental observation of a bent nanotube in a high-resolution transmission electron microscope (HRTEM), see Figure 2*a*. In order to simulate the bent shape, molecular dynamics simulations were carried out in which a nanotube was bent in small increments while its ends were held fixed (8). Because of the number of atoms involved, direct ab initio simulations were impractical at the time, and classical molecular dynamics was used insted. In order to simulate properly the complex interactions between the carbon atoms, a many-body potential (9, 10) was used that accurately reproduces the lattice constants, the binding energies, and the elastic

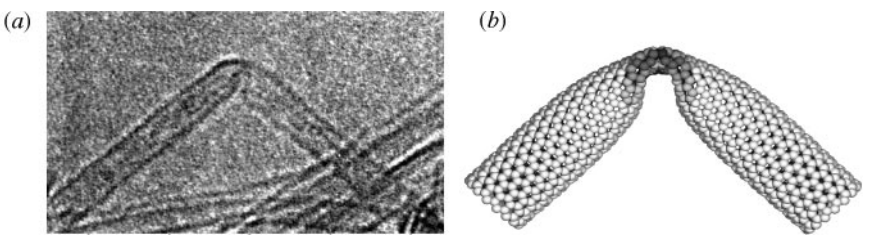

Figure 2 (*a*) HRTEM image of kink structures formed under mechanical stress in nanotubes with diameters of 0.8 and 1.2 nm. (*b*) Atomic structure of a single kink obtained in the computer simulation of bending of the single-walled tube with diameter of ∼1.2 nm. The shading indicates the local strain energy at the various atoms. From Reference (8).

constants of both graphite and diamond. These simulations reproduced well the overall shape of the bent nanotube, as shown in Figure 2*b*, and also predicted that the bending is highly reversible. This was subsequently observed in experiments (11) that used a NanoManipulator, which is a novel atomic-force microscope (AFM) controlled by a three-dimensional mouse with force feedback.

An important question from the point of view of simulations is whether a continuum model of nanotube deformations can be used instead of the much more costly atomistic simulations. This is particularly important for wide nanotubes or nanotube ensembles, where the number of atoms can be very large. In fact, an explicit comparison with simulations has shown that the well-known shell model of macroscopic continuum mechanics can quantitatively predict the onset of buckling or twisting modes, despite the fact that nanotubes are only $\sim$1 nm wide (12). Furthermore, continuum mechanics provides a general classification of the expected deformation modes. However, for very large bending angles, the distortions in the nanotube shell are large enough that rebonding can occur. This is the explanation advanced for the observed 10^2 reduction in conductivity upon deflecting a nanotube with an AFM tip (13, 14). Rebonding was also observed in simulations of severe compression or bending by tight-binding or localized orbital methods (15, 16).

Tensile Strength of Nanotubes

It has long been assumed that nanotubes are exceptionally strong because graphitic planes can support very large tension. However, because breaking and reforming of bonds at large strains is inherently a microscopic process, detailed atomistic simulations are necessary to examine the strength limits of nanotubes. In order to identify the first stages of the mechanical yield of carbon nanotubes, ab initio and classical molecular dynamics simulations were performed at high temperatures so that defect formation could be observed during the simulation time scales, which are of the order of tens of picoseconds for quantum molecular dynamics and several nanoseconds for classical dynamics. The ab initio simulations used the real-space multigrid method, which incorporates multilevel convergence acceleration and multigrid preconditioning at all length scales (17, 18). The classical molecular simulations utilized the many-body carbon potential mentioned above.

The simulations uncovered the dominant strain release mechanisms, as well as their energetics (19). Beyond a critical value of the tension, the system releases its excess strain via a spontaneous formation of topological defects. The first defect to form corresponds to a 90° rotation of a carbon-carbon bond about its center, the so-called Stone-Wales transformation (20), which produces two pentagons and two heptagons coupled in pairs (5-7-7-5) (Figure 3). Static calculations under fixed dilation show a crossover in the stability of this defect configuration with respect to the ideal hexagonal network. It is observed at about 6% tensile strain in (5,5) and (10,10) armchair tubes. This implies that the (5-7-7-5) defect is effective in releasing the excess strain energy in a tube under tensile strain.

The appearance of a (5-7-7-5) defect can be interpreted as the nucleation of a degenerate dislocation loop in the planar hexagonal network of the graphite sheet (19, 21, 22). The configuration of this primary dipole is a (5-7) core attached to an inverted (7-5) core. Therefore, the (5-7) defect behaves as a single edge dislocation in the graphitic plane. Once formed, the (5-7-7-5) dislocation loop can ease further relaxation by separating the two dislocation cores, which glide through successive bond rotations. This corresponds to a plastic flow of dislocations and gives rise to ductile behavior, as shown in Figure 3. Alternatively, larger defects may be nucleated from the (5-7-7-5) defect, leading to crack extension. The plastic flow changes the index of the nanotubes, potentially leading to metal-semiconductor junctions that could be used in novel device structures (see below).

Carbon adatoms deposited on nanotubes can also induce plastic transformations when a nanotube is subject to high strain conditions (23). Briefly, the adatoms, which are mobile at moderately high temperatures, coalesce into addimers, which can incorporate into the graphitic structure under high strain conditions by forming a novel (7-5-5-7) defect. Subsequent transformations, which need to be induced by high strain, can lead to the formation of metallic quantum dots in zigzag nanotubes (23).

The knowledge of the dominant strain-release mechanism enables investigations of the thermodynamic limit of strength, as well as of kinetic effects. The formation of the bond-rotation defect becomes energetically favorable when the total energy of a strained nanotube is lowered by its formation. The formation energy of the defect is defined as the difference between the total energies of a perfect nanotube and one with a defect. Figure 4*a* shows the formation energy as a function of strain for a (5,5) carbon nanotube and a graphene sheet subject to static strains of up to 15% (19, 24). It is clear from the figure that armchair nanotubes are thermodynamically stable up to 5 to 6% and that this value is only weakly dependent on tube diameter. Up to this thermodynamic limit, the nanotube will only deform elastically. Beyond it, the response depends on the kinetic barrier. This barrier (activation energy) for the formation of the bond rotation defect is shown in Figure 4*b* as a function of strain. Given the large size of the activation energy, the nanotube will deform elastically in a much greater strain regime. The strength of the nanotube becomes even greater if the variation with chiral angle is considered (22, 24, 25). The variation of stability with the chiral angle can be explained by examining the limiting cases. When strain is applied to armchair nanotubes, the rotating bond is originally perpendicular to the strain axis and becomes parallel when the defect is formed. This results in a slight release of the strain. In zigzag nanotubes, however, the rotating bond forms a 120° angle with the strain axis before and after the rotation, so there is no obvious gain (22). Curvature effects modify this argument somewhat, but it remains valid (22). Indeed, as can be seen in Figure 4*c*, the formation energy of the bond-rotation defect remains positive up to about 10% for zigzag nanotubes, indicating much greater thermodynamic strength. However, the activation energies in zigzag nanotubes remain similar to the energies in the armchair nanotubes.

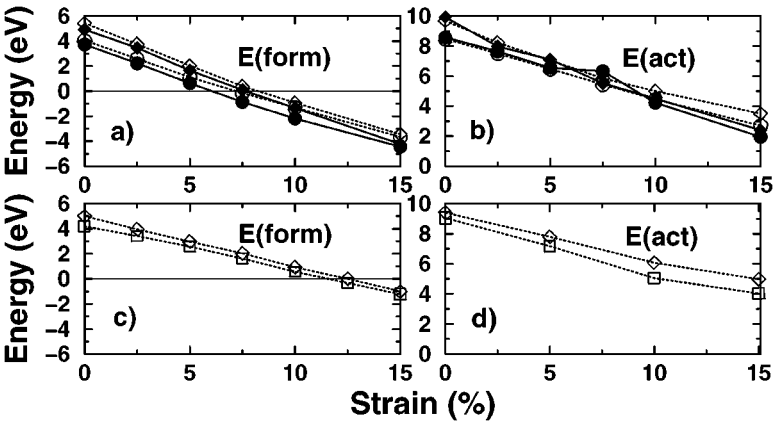

Figure 4 Formation and activation energies of the bond rotation defects as a function of strain for armchair (*a–b*) and zigzag (*c–d*) nanotubes. Circles and squares correspond to (5,5) and (17,0) tubes, and diamonds correspond to graphene sheets under transverse and longitudinal strains, respectively. Ab initio results are represented by solid symbols; tight-binding results are shown by hollow symbols and are connected by dashed lines. Adapted from Reference (24).

Subsequent experiments (26, 27) have found that nanotubes fail at strains of up to a little over 5%. Both theoretical calculations (28) and experiments (29) measuring the Young modulus of nanotubes give an exceptionally large value of over 1 TPa (normalized to the density of graphite), thus confirming that nanotubes are among the strongest materials known. Indeed, a direct measurement of breaking strengths of nanotube "ropes" gave values ranging up to 52 GPa (27). The above measurements were performed at room temperature. However, perfect nanotubes should be much stronger because the activation energies are so high. Indeed, a simple estimate based on the Arrhenius expression $\Gamma \propto N_{\text{bonds}}\, \overline{\nu} \exp(-E_{act}/k_B T)$ with $\overline{\nu} \simeq 10^{13}$ gives a negligible rate of defect formation at room temperature. It is thus likely that the nanotube samples used in these experiments contained defects. As the quality of growth and processing of nanotubes increases, the maximum strength of nanotube bundles should also increase.

Strain and Chemical Reactivity

Molecular modeling and tight-binding calculations have also been used to explore whether kinks and other regions of high curvature induced by mechanically deforming nanotubes can act as sites of enhanced chemical reactivity (30). In these calculations, single-walled (17,0) and (10,10) nanotubes were bent and twisted, and the resulting structures were obtained by minimizing the energy as given by a classical force expression. The binding energy for hydrogen chemisorption to single carbon atoms on the distorted structures, predicted from the classical force

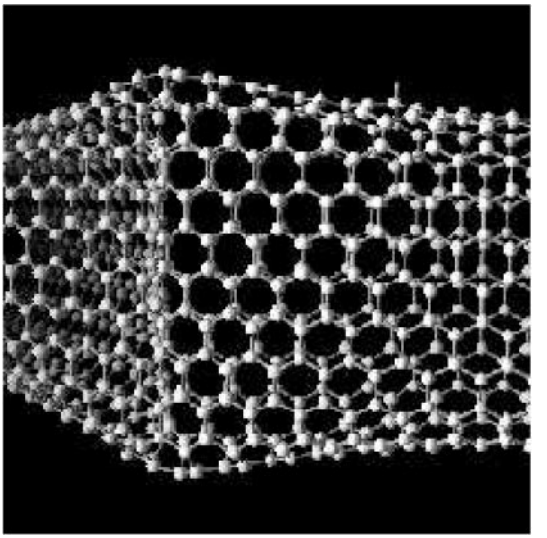

Figure 5 Molecular model of a kinked (17,0) nanotube. A chemisorbed hydrogen is apparent at the upper right of the figure (30).

expression, was then used as a metric for chemical reactivity. Illustrated in Figure 5, for example, is the predicted atomic structure near a kink in a bent (17,0) nanotube as viewed from the back of the kink. The nanotube flattens along the front and back of the kink, and there is a ridge of atoms along the kink top and bottom. This ridge is raised at the center of the kink, and the angles of the three bonds associated with the atom of the ridge apex are close to tetrahedral. The molecular modeling studies predict that a hydrogen atom can be more strongly bound to the apex carbon atom by 1.6 eV relative to chemisorption at an undistorted region of the nanotube. This enhancement in binding energy drops off smoothly for the carbon atoms along the top of the ridge, falling to an enhancement of 0.25 eV for the sites five atoms from the apex. This increase in binding energy was found to correlate with a decrease in atomic cohesive energy, as predicted both by the classical force expression and tight-binding calculations. Hydrogen atom binding was found to be weaker relative to an undistorted tube for sites along the back and front of the kink. At the back of the kink, the nanotube is under tensile hydrostatic stress, and subsequently the tetrahedral bond angles required for strong chemisorption are more difficult to form compared with an undeformed nanotube. At the inside of the kink, the nanotube structure is deformed such that carbon atoms are distorted toward the interior of the nanotube, leading to an incorrect geometry for binding hydrogen atoms to the outside of the tube.

Enhanced chemical reactivity at regions of large distortion on nanotubes, as inferred from the stronger hydrogen binding energies at kinks, has been supported by

experimental observations by Ruoff and co-workers (30). In these experiments, multi-walled nanotubes were placed along a polymer substrate containing V-shaped ridges, and dilute nitric acid was introduced into the system. Scanning electron microscopy showed significant etching of the nanotubes along the top of the substrate ridges where the high curvature presumably induced kinks in the nanotubes. Although this is indirect proof, the observation of enhanced etch rates supports the connection between enhanced chemical reactivity and large distortions of nanotubes predicted by the calculations.

Modeling of Nanotube-Based Composites

Nanotubes are important target components of nanoscale fiber-reinforced composites for mechanical and thermal management applications, owing to their large tensile modulus and high thermal conductivity, together with an apparent ability to bridge and heal cracks (31, 32). To be successfully used in nanocomposites, however, critical processing and structural challenges must be met. These challenges include using high–aspect ratio structures that are well dispersed in polymer matrices, controlling fiber alignment, and maintaining good thermal coupling and load transfer between the nanotubes and matrix. The need for well-dispersed, high–aspect ratio nanotubes has been met experimentally through continuing improvements in growth conditions and sonication of nanotube bundles, and polymer alignment via applied strain has been demonstrated (33). Experimental measurements of enhancements in the elastic modulus of polymers with the addition of a few percent nanotubes (32, 34), together with apparent shifts in Raman frequencies for nanotubes dispersed in loaded polymer matrices (31, 35–37), suggest that load transfer can be strong enough to make these systems attractive for structural applications. However, the specific mechanism(s) by which load is transferred between polymer matrices and nanotubes is not clear. Determining this mechanism (and ways to enhance it) has been a central focus of recent molecular mechanics modeling studies.

Lordi & Yao used force-field-based molecular mechanics to model the interactions between nanotubes and several polymers (38). The polymers were chosen to represent experimental composite systems for which both strong and weak adhesions between the matrix and nanotubes have been measured. They report interfacial binding energies between 5.9 and 12.5 meV/Å^2, and maximum frictional stresses for sliding nanotubes within single polymer chains of between 29.3 and 139 MPa. These values can be compared with the interfacial energy and sliding stress for two graphite planes, which they report as 8.25 meV/Å^2 and 31.8 MPa, respectively. Interestingly, little correlation was found between interfacial energy and maximum shear stress for the polymers studied. These studies indicated that hydrogen bond interactions between the polymers and nanotubes make the most significant contributions to the binding energy and suggest that helical polymer conformations in which chains can wrap around nanotubes are essential to producing strong nanotube-polymer interactions.

In related studies, Frankland et al. used force-field expressions that both assume a united-atom approximation and explicitly include hydrogen atoms to model single-shelled (10,10) nanotubes in crystalline and amorphous matrices representing polyethylene (39, 40). This system was chosen because of its simplicity and not because it is necessarily experimentally accessible or would make a composite with particularly strong interfacial interactions. Nonbonded tubule-polymer interactions, as well as chemical crosslinks between nanotubes and the matrix, were considered. For the nonbonded tubule-polymer interactions, critical shear stresses needed to slide the tubule through the matrix ranged from 0.7 MPa for the amorphous matrix/united-atom potentials to 2.8 MPa for a crystalline matrix/explicit hydrogen model. Assuming a fiber strength of 50 GPa for the nanotubes, these critical shear stress values imply that lengths exceeding about 25 μm would be needed for significant load transfer between the matrix and tubules. Molecular dynamics simulations were also used to model loading strain for composites containing (10,10) nanotubes of varying lengths. The largest system modeled contained a 100 nm long nanotube in a united-atom/amorphous polyethylene matrix. Consistent with the critical shear stresses determined from the pull-through simulations in each of these loading simulations, the nanotubes were released from the matrix starting at their ends and subsequently regained their initial length.

Simulations by Frankland et al. (40) also predicted that chemical crosslinks between tubules and matrices involving less than 1% of carbon atoms on a single-walled tubule can increase critical shear strengths by a factor of about 40. With these values, corresponding critical lengths (again assuming a fiber strength of 50 GPa for the nanotubes) drop from $\sim$25 to 0.6–2.0 μm. Preliminary calculations using an empirical potential predict that this relatively small level of functionalization does not significantly reduce the tensile modulus of a (10,10) nanotube. This result, together with the composite modeling, suggests that chemical functionalization leading to matrix-tubule crosslinking may be an effective mode for enhancing load transfer in these systems without sacrificing the elastic moduli of tubules.

ELECTRONIC PROPERTIES OF CARBON NANOTUBES

Carbon nanotubes are one-dimensional structures that exhibit remarkable electronic properties depending upon their diameter and helicity. As explained by Hamada et al. (41), the salient electronic properties of nanotubes may be understood in terms of a simple tight-binding model. For instance, consider an infinite graphene sheet. Using a nearest-neighbor Hamiltonian for the electron hopping between the π and π^* bands, with coupling $V_{pp\pi} = -2.75$ eV, the two-dimensional band structure of the sheet is given by

$$\epsilon_{\pm}(\mathbf{k}) = E_F \pm V_{pp\pi}\sqrt{3 + 2\cos\mathbf{k}.\mathbf{a}_1 + 2\cos\mathbf{k}.\mathbf{a}_2 + 2\cos\mathbf{k}.(\mathbf{a}_1 - \mathbf{a}_2)}, \qquad 1.$$

where $\mathbf{k}$ is any two-dimensional wave vector within the hexagonal Brillouin zone and ($\mathbf{a}_1$, $\mathbf{a}_2$) are the base vectors for the unit cell.

Carbon nanotubes are formed when the graphene sheet is rolled up into a cylinder in such a way that the carbon atoms connect seamlessly with each other. This implies that carbon atoms whose relative position vector is $\mathbf{C} = n\mathbf{a}_1 + m\mathbf{a}_2$ must overlap, which in turn gives the condition $\mathbf{C}.\mathbf{k} = q\,2\pi$, where q is an integer. This relation defines a set of parallel lines with a relative separation $\mathbf{C}/2\pi$. Schematically, these lines are represented for three types of nanotubes with helicity indices (n, m) (Figure 6). The K point $[\mathbf{k}_K = (\mathbf{a} - \mathbf{b})/3]$ is the point where the π and π^* bands of a graphene sheet meet, defining the Fermi energy. Depending on whether a line intercepts or misses the K point, the resulting nanotube will be either metallic or semiconducting. Thus tubes for which $(m - n)$ is divisible by three will have a finite density of states at the Fermi level and will therefore be metallic. In particular, all armchair $n = m$ nanotubes are metallic, whereas only a third of the $m = 0$ zigzag nanotubes have metallic characteristics.

Although this model is relatively simple, it works remarkably well. There are, however, limitations that result from a possible mixing between the in-plane σ and out-of-plane π orbitals. These orbitals are, of course, orthogonal for a simple graphene sheet but may be somewhat mixed for highly curved systems. As a general rule, this mixing can be neglected for nanotubes with radii greater than 10 Å. For nanotubes with radii in the range of 2.5 to 10 Å, a small band gap decreasing with the second power of the radius appears in all but the armchair nanotubes. For nanotubes with even smaller radii—some of which have been synthesized recently—the simple model presented here is no longer valid, and more fundamental, first-principles calculations are needed to adequately describe the

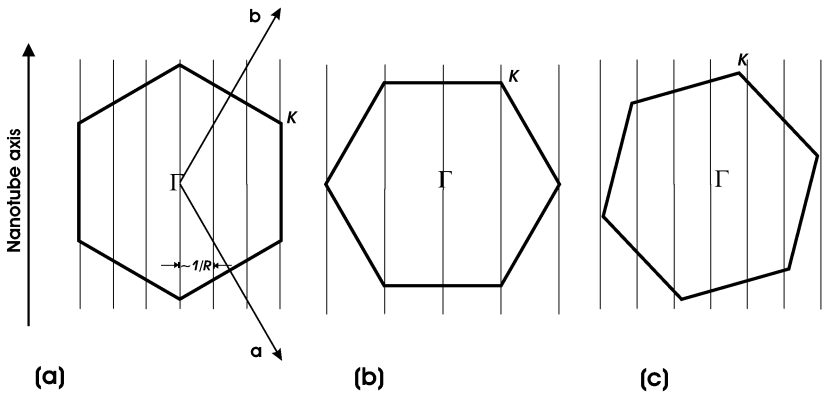

Figure 6 Schematic representation of the first Brillouin zone of a single graphene sheet. The lines $\mathbf{k}.\mathbf{C} = q2\pi$ are drawn for (*a*) an armchair (3,3), (*b*) a zigzag (3,0), and (*c*) a chiral (4,2) nanotube. The K point of the Brillouin zone is the crossing point of the π and π^* bands. The nanotube will be metallic only if one of the lines intercepts this point. From the drawing, this condition will only be met for certain orientations and spacing ($\sim R^{-1}$) of the set of lines.

electronic properties of these very-small-diameter nanotube systems (42). Furthermore, single-walled nanotubes usually self-assemble in bundles called ropes owing to van der Waals attraction. The intertube interactions introduce small pseudogaps in ropes of nominally metallic tubes (43, 44). Another issue is the emergence of one-dimensional weak localization, due to a correlated-electron ground state in nominally metallic nanotubes at very low temperatures—the Luttinger liquid (45–48). Signatures of the Luttinger liquid have been seen in low-temperature transport experiments, where a characteristic power-law dependence of the differential quantum conductance was observed (49, 50).

Structural deformations have significant effect on the electronic properties of nanotubes. It was shown early on that uniaxial stress, while not greatly affecting the band structure of armchair nanotubes, significantly alters the band structure of zigzag nanotubes (51). In fact, it is possible to use the simple analytical relations for the π band structure of graphene to derive the strain-induced changes in the electronic structure of nanotubes. The resulting relations predict a transition from semiconducting to metallic behavior as a function of strain and vice versa (51, 52). The same effects are obtained in more sophisticated calculations, with only some quantitative modifications.

STM Images and STS Spectra of Carbon Nanotubes

Local probe techniques are excellent tools for understanding the intrinsic properties of nanoscale systems such as carbon nanotubes. Most important are scanning tunneling microscopy (STM) and spectroscopy (STS), two among the very few experimental techniques that allow for a determination of nanotube helicity (53). The helicity may be deduced from two independent measurements: (*a*) the nanotube diameter

$$D = \frac{\sqrt{3} d_{CC} \sqrt{n^2 + m^2 + mn}}{\pi}, \qquad 2.$$

with $d_{CC} = 1.41$ Å being the carbon-carbon bond distance, and (*b*) the pitch angle

$$\phi = \arctan \frac{(n - m)}{\sqrt{3}(n + m)}, \qquad 3.$$

which is the angle that a zigzag chain of atoms makes with the nanotube axis. Both quantities are determined through combined STM and STS measurements.

The first reported STM experiments on multi-walled carbon nanotubes date back almost a decade (54, 55). At that time, Ge & Sattler (56) recorded an STM image of a multi-walled nanotube that displayed an atomically resolved pattern affected by the two outermost layers of the tubes. Other groups subsequently succeeded in obtaining atomically resolved images, and in 1996, Lin et al. (57) accurately determined the chiral angle of the outermost layer of a multi-walled nanotube. The first measurements on single-walled nanotubes date back to 1994 (58). Four years later, the groups of Lieber and Dekker independently succeeded

in recording atomically resolved images on numerous individual (59, 60) and in-rope (60) nanotubes. At the same time, Maruyama et al. and Hassanien et al. reported the first atomically resolved images of single-walled nanotubes synthesized by the arc discharge method (61, 62). More recent studies have investigated ion irradiation-induced atomic vacancies in nanotube walls (63), through an in situ study of nanotube defect structures. Striking images of intramolecular nanotube junctions and the corresponding topological defects have also been measured (64).

For perfect nanotubes, the pitch angle (or chirality) of a carbon nanotube may be determined, provided that atomic resolution is maintained over a sufficiently large portion of the sample during the scan. However, even with very good spatial resolution (typically smaller than 0.5 Å), extracting reliable information from experimental images is not an easy task. Indeed, the pitch angle is strongly affected not only by distortions induced by a torsional twist (65), but also by the lateral distortion due to the cylindrical shape of the nanotube (58, 66), which is the result of the tunneling current flowing from the tip to the nanotube via the shortest path (i.e., perpendicular to the nanotube surface), so that the recorded image is the result of a projection onto the scanning plane (66). This effect is simple enough to correct if the tube-tip height and the radius are known. Successful corrections of this type have been reported in the literature (67).

Aside from geometrical distortions, low-bias STM images contain a number of interesting features. For instance, even long and defect-free nanotubes rarely display the perfect hexagonal pattern one would expect from the corresponding ball and stick models of the tubes (68). This is independent of the quality of the experiments and is due to the fact that the low-positive (negative) bias images are not faithful representations of the total electron density but of a superposition of quantum states located just below (above) the Fermi energy. For example, a horizontal striped pattern is often observed in images. The origin of this feature is to be found in the electronic properties of the nanotube, as theoretically reproduced in Reference (66) and nicely explained by Kane & Mele (69). The main conclusion is that for semiconducting nanotubes only the superposition of both the positive and negative bias images creates a faithful representation of the underlying atomic structure, as beautifully demonstrated by the experiments of Clauss et al. (68).

Given the difficulties of extracting accurate information from what are sometimes tricky experimental images, it has become clear that simple but robust theoretical methods are needed to aid in the interpretation of the STM images. A number of different approaches have been introduced involving either the wave-packet scattering (70, 71) or tight-binding approaches (66, 69), as well as the more computationally intensive ab initio calculations (72, 73). A semi-empirical method for computing the tunneling current was introduced early on (74) and first applied to curved graphitic systems by Meunier & Lambin and Meunier et al. (66, 75). Given its simplicity, we review the basic features of this approach here.

The tunneling current between a metallic tip and a graphitic substrate is computed using a general first-order expression of the tunneling current between the tip (t) and the substrate (s):

$$\mathcal{I} = (2\pi)^2 \frac{e}{h} \int_{-eV}^{0} dE \sum_{i,i' \in t} \sum_{j,j' \in s} v_{ij}\, v^*_{i'j'}\, n^t_{ii'}\left(E^t_F + eV + E\right) n^s_{jj'}\left(E^s_F + E\right), \quad 4.$$

where V is the tip-sample bias potential ($e > 0$), the n_{ij} are the matrix elements of the density operator, E_F are the Fermi levels of the unperturbed systems, and v_{ij} are the tip-sample coupling elements. The coupling elements are parameterized and adjusted in such a way as to fit the experimental data on mono- and bilayered graphite. The tip is described by a single s-orbital atom, as in the Tersoff-Hamann theory (76), and its density of states is assumed to be a Gaussian. It is sufficient to model the nanotube with a π-electron tight-binding Hamiltonian with constant first-neighbor interactions. The diagonal and off-diagonal elements of the nanotube Green's function can be calculated using a standard recursion algorithm. The matrix elements coupling the tip apex atom to the atoms of the nanotube are Slater-Koster sp-like hopping terms, which decay exponentially with the separation distance and are weighted to select the carbon atoms closest to the tip. However, one must keep the off-diagonal elements of the density operator ($n_{ii'}$) for a correct simulation of the images. In the absence of those terms, key features such as the current intensity on chemical bonds and the complementary nature of the positive and negative bias images are not reproduced.

The utility of this approach has been checked by comparison with other semi-empirical (69) and ab initio (72) calculations. It has been used to model perfect (66), finite-sized (75), defective (66, 77, 78), and multi-walled (79) nanotube systems. As an example, Figure 7 shows simulated STM images of a carbon nanotube taper. There is currently considerable interest in the properties of such tapered systems for applications as local scanning probe tips and as electron field emitters.

STS measurements are performed by keeping the STM tip stationary above the nanotube, switching off the feedback mechanism, and recording the current as a function of the voltage applied to the sample. The differential conductances (dI/dV) of the measured current-voltage curves are known to compare very well with the density of states (DOS) of the sample, for voltage amplitudes up to at least 0.75 V.

The first task of STS measurements was to confirm the electronic properties of nanotubes. This has been performed by two independent groups (59, 60) who showed that the differential conductance curves display all the predicted major features, the most striking of these being undoubtedly the typical van Hove peaks characteristic of nanotube DOS. Even more subtle features such as the presence of small gaps in the metallic plateau (80) have been observed. This phenomenon is attributed to $\sigma - \pi$ hybridization occurring in highly curved graphitic networks.

STS measurements of nanotube systems have progressed to such a stage that they can now be used for routine (81) and systematic (82) determination of the nanotube radii. This method is based on the following approximate relations

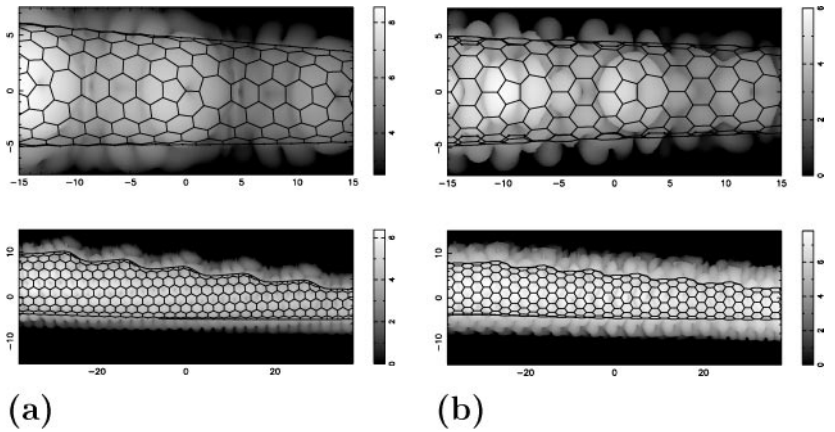

Figure 7 Calculated constant current 0.5 V STM image of a (*a*) (5,5)/(6,6)/(7,7)/(8,8)/(9,9)/(10,10) armchair taper and (*b*) (9,0)/(10,0)/(11,0)/(12,0)/(13,0)/(14,0)/(15,0) zigzag taper. The tip height is represented by the grayscale index. The pentagonal rings protrude from the top view image and the hexagonal lattice is not clearly rendered from either the top or the side views. All distances are in Å.

(83, 84): For semiconducting nanotubes [for which $(m - n)$ is not a multiple of 3] the band gap is given by

$$E_g = \frac{2\gamma_0 d_{CC}}{D}, \qquad 5.$$

whereas for metallic nanotubes, the width of the metallic plateau, defined as the distance between the first van Hove singularities located on each side of the Fermi energy, is given by

$$E_p = \frac{6\gamma_0 d_{CC}}{D}. \qquad 6.$$

When available, further van Hove singularities can be used to refine the radius determination. When STS is used together with STM, a complete determination of nanotube structure is thus possible. We should point out that it is very difficult to accurately determine the nanotube diameter solely from STM images because of tip-shape convolution effects (70, 71).

In addition, because STS is inherently a local probe technique, it can be used to localize key features such as resonant states at nanotube tips both spatially and energetically (85, 86). Associated with theoretical calculations, this type of measurement permits the precise determination of the underlying atomic structure. More fundamentally, STS has been successfully used to image the spatial distribution of electrons and therefore visualize wave functions of quantized energy levels characteristic of finite-sized carbon nanotubes (87).

Conductance of Carbon Nanotube Systems

With advances in fabrication, there has been a significant upsurge in quantum transport research, especially in nanostructured systems (88). In particular, carbon nanotube systems have acted as a convenient test bed or laboratory for exploring transport properties at the nanometer scale.

At nanometer distances, electrons can move ballistically through the device without any scattering. For ballistic transport, the relation between the current (I) and the voltage (V) is $I = GV$, where G is the quantum conductance. The famous Landauer formula (89) relates G to the transmission coefficient $\mathcal{T}$ via

$$G = (2e^2/h)\mathcal{T}. \qquad 7.$$

Because a metallic nanotube has two extended electron bands crossing at the Fermi level, it should behave as an ideal two-channel ballistic conductor: Every electron injected into it should pass through without scattering. The theoretical conductance should thus be a constant $G = 2 \times G_o = 2 \times (2e^2/h) \approx 2 \times (12.9\ K\Omega)^{-1}$. In principle, at larger electron energies, the electrons are able to probe additional bands, which would give a corresponding increase in G. In practice, the propagating electrons will be scattered by lattice defects and eventually by phonons, and the injection of electrons must proceed through contacts, which can act as strong scatterers. In addition, Luttinger liquid effects can substantially reduce conductance in the limit of weak coupling to the leads.

A calculation of quantum conductance requires the evaluation of transmission probability through an open system, consisting of a conductor and two or more leads. The general formalism of quantum transport is well described elsewhere (90, 91). A variety of techniques has been used for nanotubes (92–105), which all build on Green's function or related scattering or transfer operators. We outline below a relatively simple and efficient procedure to compute the quantum conductance within the tight-binding methodology (100, 101), which can also be adapted to ab initio calculations (105).

In order to calculate the Green's function matrix of the conductor with open boundary conditions, one can partition the system into a left lead (L), a conductor (C), and a right lead (R), for example by using a local-orbital basis. For orthogonal orbitals, the Green's function equations become

$$\begin{pmatrix} G_L & G_{LC} & 0 \\ G_{CL} & G_C & G_{CR} \\ 0 & G_{RC} & G_R \end{pmatrix} = \begin{pmatrix} (\varepsilon - H_L) & H_{LC} & 0 \\ H_{CL} & (\varepsilon - H_C) & H_{RC} \\ 0 & H_{CR} & (\varepsilon - H_R) \end{pmatrix}^{-1}. \qquad 8.$$

Here, G and H with the appropriate indices refer to the Green's functions and the Hamiltonians, respectively, and $H_{\{L,R\}C}$, etc. denote the coupling terms. One can separately solve for the self-energies of the left and right leads, which assume the form

$$\Sigma_{\{L,R\}} = H^{\dagger}_{\{L,R\}C} G_{\{L,R\}} H_{\{L,R\}C}. \qquad 9.$$

The coupling Hamiltonians $H_{\{L,R\}C}$ are very short-ranged when local orbitals are used, and the Green's functions for the semi-infinite leads can be obtained for any periodic lead by recursively doubling the period (106, 107). Using the self-energies, the Green's function for the conductor becomes

$$G_C = (\epsilon - H_C - \Sigma_L - \Sigma_R)^{-1}. \qquad 10.$$

One can then show (108, 109) that the transmission function is

$$\mathcal{T} = \mathrm{Tr}\big(\Gamma_L G_C^R \Gamma_R G_C^A\big), \qquad 11.$$

where $\Gamma_{\{L,R\}}$ describe the coupling of the conductor to the left/right leads and are given by

$$\Gamma_{\{L,R\}} = \mathrm{i}\left[\Sigma^r_{\{L,R\}} - \Sigma^a_{\{L,R\}}\right]. \qquad 12.$$

These equations are valid in both the Landauer approach and the non-interacting limit of the more sophisticated Keldysh non-equilibrium Green's function formulation.

Chico et al. (94) pioneered the conductance studies of nanotubes by investigating the conductance of defective tubes and tube junctions using the π-orbital tight-binding model. They have shown that scattering by single vacancies reduces but does not eliminate the conductance at the Fermi level and that the magnitude of the reduction is inversely proportional to the diameter of the nanotube, as one would expect. Furthermore, they have shown that in certain metallic nanotube junctions, connected by pentagon-heptagon pairs (110), the conductance is completely suppressed for symmetry reasons.

Disorder effects are an important issue in one-dimensional transport. White & Todorov (111) predicted that in contrast to normal metallic nanowires, where electrons can become localized because of the one-dimensional nature of the system, conduction electrons in metallic armchair nanotubes experience an effective disorder averaged over the tube circumference, leading to electron mean free paths that increase with nanotube diameter. This increase results in exceptional ballistic transport properties and localization lengths of the order of hundreds of nanometers and more, as has been observed experimentally (6). Similarly, theoretical studies by Anantram & Govindan (97) have shown that weak uniform disorder does not significantly affect conductance near the band center. More recently, the effects of disorder on the conducting properties of metallic and semiconducting carbon nanotubes have been addressed both theoretically and experimentally by McEuen et al. (112). They demonstrated that the mean free path is much larger in metallic tubes than in doped semiconducting tubes and showed that this result can be understood theoretically if the disorder potential is long ranged.

Experimentally, the quantized nature of transport through carbon nanotubes was first investigated by Frank et al. (113), who observed that the conductance of multi-walled carbon nanotubes is quantized and that nanotubes do indeed behave as ballistic conductors. They measured the electron transfer between liquid

mercury and a multi-walled nanotube, obtaining a highly reproducible result of a single conductance quantum G_o. Although this difference between the measured and theoretically predicted value of $2G_o$ was considered puzzling, it is now believed to be due either to a back-scattering mechanism from the metal (114) or to possible inter-wall interactions within the multi-walled nanotubes (102, 115). The most recent measurements (116, 117) on well-contacted metallic nanotubes obtain values close to $2G_o$, which is consistent with band structure predictions.

Because specific defects and impurities introduce different scattering and bound states, their effects on conductance differ significantly. As expected, B doping mainly affects the lower part of the metallic plateau, as does the vacancy, whereas N doping reduces conductance only in the upper part (118). More complex defects, such as the pentagon-heptagon pair, reduce conductance at both ends of the plateau. Very recently, resonant electron scattering by structural defects has been observed, although it has not been possible to resolve the structure of the defects (119). Molecular adsorption can also have substantial effect. In particular, the effects of oxygen adsorption on conductivity are dramatic, converting originally semiconducting nanotubes into apparent metals (120), probably by hole doping (121). Substantial changes in the electrical properties of nanotubes have also been observed upon adsorption of NO_2 or NH_3, and this effect could be used in ultrasensitive gas sensors (122).

For changes in conductance induced by mechanical deformations, experiments (123) have shown that individual carbon nanotubes, which were deposited on a series of protruding electrodes, could be classified into three groups on the basis of their electrical behavior: (*a*) non-conducting at room temperature and below, (*b*) conducting at all temperatures, and (*c*) partially conducting. The last class represents nanotubes that are conducting at a high temperature but at a low temperature behave as a chain of quantum wires connected in series. It has been argued that the local barriers in the wire arise from bending near the edges of the electrodes. Loss of conductance was observed when a single-wall nanotube was severely deformed by an AFM tip (13) and also in the final stages of breakage of a multi-walled nanotube (124). However, in the latter case, the initial pulling had little effect on the resistance.

There have been a number of theoretical investigations of the quantum conductance of bent nanotubes, of both infinite (101) and finite sizes (13, 125, 126). In general, the calculations have shown that the conductance of armchair nanotubes is relatively insensitive toward deformations: Very large distortions are required before substantial changes in the conductance occur. For chiral nanotubes, however, the local strain at the kink site opens a small gap in the electronic spectrum very early on. This extreme sensitivity could be used in switches or strain sensors. Figure 8 shows the conductances of bent nanotubes of infinite length, which illustrates well the general trends. For nanotubes of finite lengths, the conductances consist of closely spaced peaks corresponding to the discrete energy levels of the finite system, which merge into the continuum limit as the length of the nanotube segment is increased. The distribution of these peaks is length dependent and may

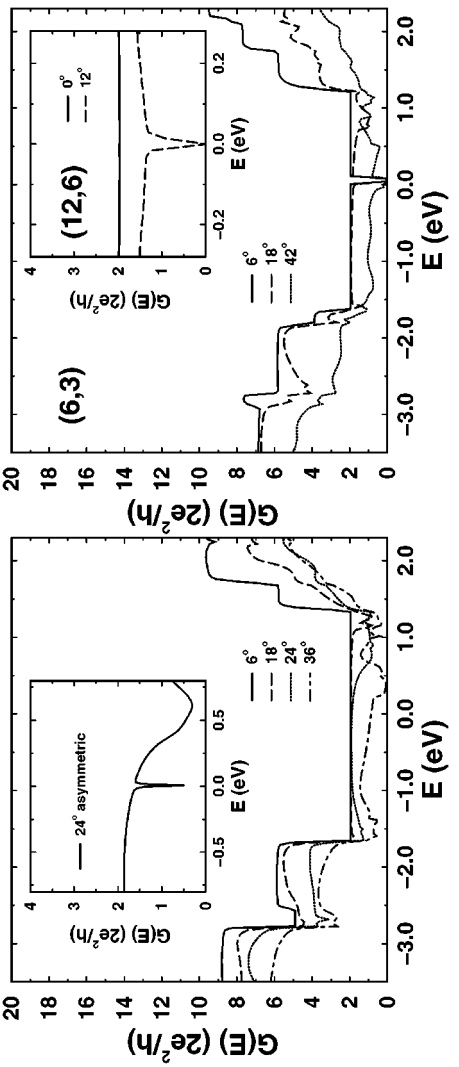

Figure 8 Conductances of symmetrically bent (5,5) armchair and (6,3) chiral nanotubes. Insets: conductances of a (5,5) tube with an asymmetric bend of 24°, and of a bent (12,6) chiral nanotube for $\theta = 0°$, 12°. The Fermi energy is taken as reference.

be understood in terms of the band structure of the nanotubes. If an AFM tip is used to facilitate nanotube bending, then a local rebonding near the kink can also occur (13, 14), which alters the conductance.

Using these theoretical considerations, one can tentatively interpret the experimentally observed three classes of behavior (123) arising from (*a*) semiconducting nanotubes, (*b*) armchair nanotubes, and (*c*) chiral nanotubes. Similarly, the initial insensitivity of the multi-walled nanotube to strain might indicate that the shell(s) in contact with the electrodes had an armchair structure. However, the calculations did not consider the effects of the metal substrate and also neglected electron-correlation effects, which could further complicate the picture.

The loss of conductance owing to severe bending can be utilized in making a quantum dot in a conducting nanotube by forming two sharp bends within a short distance (127–129). The quantum dot can even be small enough to act as a single-electron transistor at room temperature (129), which opens exciting possibilities for nanoscale electronics. Additional theoretically predicted mechanisms for making nanotube-based quantum dots in semiconducting nanotubes include addimer-induced transformations under strain (23) and radial flattening of nanotube segments, which leads to metallization (130).

Nanotube-Metal Contacts

Critical to carbon nanotube-based devices is the problem of constructing a good metal-nanotube contact. As discussed above, ideal nanotube-metal devices should have contact resistances in the $K\Omega$ range. In a few recent investigations very-low-resistance ohmic contacts have indeed been achieved (116, 117). In most cases, however, carbon nanotube devices display contact resistances of the order of $M\Omega$ (6, 131–133). What is the physical origin behind the very-high-contact resistance for carbon nanotube systems? As a prototypical example, we consider the transport properties of a metallic (5,5) nanotube deposited on an Al (111) surface. In order to accurately account for the highly inhomogeneous environment of the nanowire-metal junction, and to account for the charge transfer occurring at the interface between these two dissimilar materials, an accurate self-consistent ab initio calculation was carried out (105).

One of the main characteristics of the electronic response of the nanotube-metal system is a marked transfer of charge from the nanotube to the metal, as shown in Figure 9, which allows the valence band edge of the nanotube to align with the Fermi level of the metal electrode, as expected on general grounds (134). This charge transfer, which has also been observed for other systems in both experiments (59, 131, 132) and calculations (72, 99, 134), leads to enhanced conductivity along the tube axis and gives rise to a weak ionic bonding between the tube and the metal. The conductance spectrum for the coupled nanotube is displayed in the left panel of Figure 10. Although the interaction with the metal reduces the conductance at the Fermi level by a factor of two compared with the ideal value of $2G_0$, the transmission through the system is still substantial. However, when

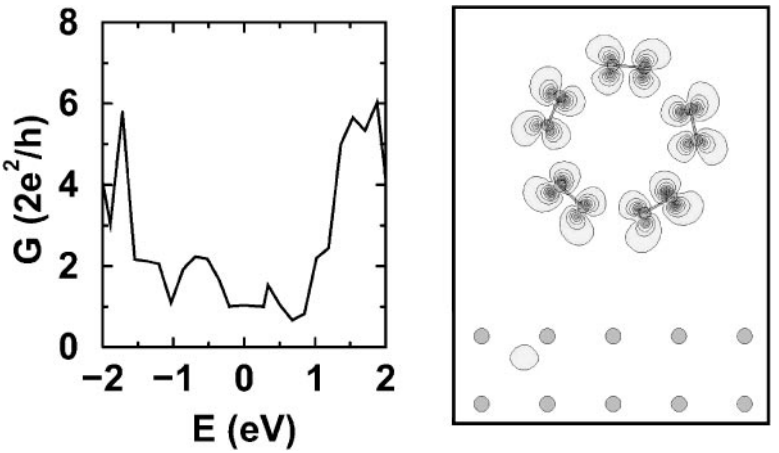

Figure 10 *Left panel*: The geometry and conductance spectrum of an infinite (5,5) nanotube deposited on Al(111). The energy zero is at the Fermi level. *Right panel*: cross section of the probability density of the electronic wavefunction corresponding to the only open eigen-channel at the Fermi level that has a sizable component on the nanotube. The other wavefunctions at the Fermi level are mostly localized on the metal.

the conductance channels, the so-called eigen-channels (135), are calculated, it turns out that in this case they separate into those that are localized in the metal and those on the nanotube itself. In particular, the eigen-channel corresponding to the plateau of conductance around the Fermi energy corresponds to the individual wavefunction, shown in the right panel of Figure 10, which is almost fully localized on the nanotube (93%). Because there is very little hybridization and intermixing between the nanotube and the metal in this channel, the electron transfer between the nanotube and the metal is inefficient in this case. This weakly distributed coupling may explain the high contact resistance observed in nanotube-metal contacts (131–133). It also explains why the measured contact resistance is inversely proportional to the contact length (6, 113, 136). Although the nanotube behaves as a ballistic conductor, the bonding characteristics in this idealized contact geometry prevent efficient electron transfer from the nanotube to the Al contact. Mechanically pushing the nanotube closer to the Al surface by a small amount ($\approx$1 Å, with an energy cost of $\approx$10 meV/atom) more than doubles the transmission efficiency between the metal and the nanotube by inducing stronger hybridization between the nanotube and the metal in the conducting channels. Alternatively, experiments have shown (133) that inducing defects in the contact region, e.g., by localized electron bombardment, drastically improves the conductance of high-resistance contacts, presumably by forcing wavefunction rehybridization.

If all contacts to a finite-size nanotube are highly resistive, the nanotube can behave as an effective quantum dot, with conductance that exhibits Coulomb blockade

behavior. Indeed, the experimental work on nanotubes in the Coulomb blockade regimes is impressive (6, 7, 137). In particular, it has been observed that conductance is higher or lower depending on whether the number of electrons in the carbon nanotubes is even or odd (137). The low-to-high peak alteration continues as a function of the applied gate voltage, and the saturation current is nonsymmetric with respect to the polarity of the bias voltage; both behaviors are indicative of an asymmetric coupling of the nanotube to the metallic leads. These interesting results may be understood by assuming the existence of spin-degenerate levels in the dot that are split, when occupied, by electron repulsion energy U. The relevant formalism (138), which is a suitable generalization of the constant interaction model (139, 140), shows that this effect is completely general and should also be present in other systems.

Hybrid junctions, in which carbon nanotubes are contacted electrically to materials with more exotic characteristics, have recently been fabricated. Among such structures, we briefly review the coupling of nanotubes to ferromagnetic and superconducting leads.

Spin-coherent transport in a carbon nanotube magnetic tunnel junction was recently investigated experimentally with two cobalt leads attached to a nanotube (141). The data showed that the nanotubes have a spin-scattering length of at least 130 nm, making them good candidates for molecular-scale magnetoelectronic devices in which both the charge and the spin degrees of freedom are utilized. The spin-coherent quantum transport through a carbon nanotube coupled to two ferromagnetic leads was examined theoretically by Mehrez et al. (142), who observed a clear spin-valve effect, characterized by a minimum resistance when the magnetization axes of the two leads are parallel and a maximum resistance when they are antiparallel. Physically, this variation in the resistance is a reflection of the differences in the majority and minority carrier concentrations in the ferromagnetic lead material.

Nanotube-superconducting junctions have been the subject of extensive experimental (143) and theoretical (144) investigations. The experimental setup consists of single-wall metallic nanotubes (SWNT) in the normal (N) state, which bridges two superconducting (S) niobium leads. By tuning the transparency of the device, clear signals of Andreev reflections (145) were detected via changes in the sub-gap resistance at $T = 4.2$ K, whereas an additional narrow peak in dV/dI emerged at $T = 2$ K. Although Andreev reflections, in which an electron propagating from the N side of a N/S junction is converted to a Cooper pair and a back-scattered hole, are well known, the emergence of an additional peak at $T = 2$ K could be viewed as a characteristic of the correlated-electron many-body Luttinger liquid (47, 50).

The theoretical analysis considered the somewhat simpler problem of a normal metal (N)-SWNT-S system because each of the two SWNT-S junctions acted independently (143). The theory combined the non-equilibrium Green's function formalism with a tight-binding model for the nanotube, representing the coupling of the nanotube to the left (N) and right (S) leads via their appropriate self-energies. The results for $T = 4.2$ K are in good, semiqualitative agreement with the

experimental results. Surprisingly, at lower temperatures, a narrow peak emerges in the calculations that are based solely on single-electron theory without the inclusion of many-body effects. A simplified analysis reveals that the origin of the peak is due to the small splitting between the electron and hole levels that occurs when a nanotube is in contact with a superconducting lead. This leads to a small peak in the differential conductance, which is washed out as the temperature is increased.

Dynamic Conductance of Carbon Nanotubes

So far, all aspects of quantum transport discussed here are based on the flow of a direct current (DC) through nanotube systems. What about the flow of an alternating current (AC)? AC conductance in a material is complicated by the presence of time-dependent fields that can take the system out of equilibrium. Under AC conditions, electrodynamics shows that the induced displacement currents need to be accounted for if the total current is to be conserved and gauge invariance maintained. Another important feature associated with the AC response is photon-assisted tunneling. In the presence of a time-varying potential, electrons can absorb photons and thereby inelastically tunnel through higher energy levels.

The dynamical response of carbon nanotubes to AC has been investigated in the wide-band limit (146). In general, dynamic effects are quite small for low AC frequencies. For larger frequencies, $0.1 \leq \hbar\omega \leq 1$ eV, there is a general reduction in the conductance because the induced displacement currents act to reduce the normal conduction current. At frequencies of more than $\approx$1 eV, this trend is reversed and the conduction is actually increased. This effect is due to photon-assisted tunneling, which places the electrons into higher energy subbands. The net result is that the conductance, after an initial decrease, is greatly enhanced. It is characterized by the emergence of an imaginary component signaling that the nanotubes have acquired a capacitive and/or inductive behavior, depending on the frequency. The relevant AC frequencies are well in the infrared to optical range, and hence it should be useful to explore future nanotube-based optoelectronic devices combined with semiconductor technology.

Nanotube-Based Devices

Nanotube-based electronics is one of the main potential uses of nanotubes. An in-depth review of this rapidly emerging field is outside of the scope of this article, and we provide only a short discussion.

The flexibility of nanoscale design and the availability of both semiconducting and metallic nanotubes enable a wide variety of device configurations. Early prototypical devices utilized the surface on which a nanotube was deposited as a gate (131, 132), but an ungated junction between a semiconducting and metallic nanotube can act as a diode (147). Junctions between two crossed nanotubes can act as rectifiers (148), and a crossed nanotube array was utilized as a random-access, non-volatile memory (149). One can also use the varying contact between a rotating nanotube on a graphite surface as a potential rheostat (150),

where the best transmission occurs when the two structures are in registry. A similar effect occurs in junctions between two overlapping nanotubes (151). In the above subsections we also mentioned nanotube-based single-electron transistors (129) and chemical sensors (122). Theoretically, negative differential resistance has been predicted for a number of nanotube-based systems, including p-n junctions and metal-nanotube-metal junctions (152). A more exotic configuration for nanoscale devices is a Y-junction, which has recently been synthesized and characterized (153, 154), as well as investigated theoretically (155, 156). A different novel application is an electromechanical actuator based on sheets of single-walled nanotubes (157), which could be used in artificial muscles.

Although a number of nanotube-based devices have been made, the production and integration of nanotube components into easily reproducible device structures presents many challenges. Recently, however, several major steps toward nanotube-based circuitry have been achieved: An array of field-effect transistors has been made by selective burning-off of metallic nanotubes in single-wall nanotube ropes (158) and logic circuits based on carbon nanotubes have been made by two groups (159, 160).

SUMMARY AND OUTLOOK

This short review has summarized the recent advances, with emphasis on theoretical developments. Nanotubes are truly exciting materials, and it is clear that the progress has been extremely rapid, as evidenced not only by the large number and quality of scientific studies, but also by the growing numbers of applications that have been proposed for these materials. This trend is only expected to increase as some of the unique and curious properties of nanotubes become clearer and the methods for their production and manipulation improve further.

Nanotubes possess extraordinary mechanical properties and are among the strongest materials known. While their ultimate strength limits are still to be reached in a laboratory, practical applications must also await the invention of methods that will produce substantial quantities of nanotubes in a suitable form. Nanotube-polymer composites are a possibility, but a process for facilitating load transfer between nanotubes and the polymer needs to be developed. The high flexibility and resilience of nanotubes points to their usefulness as tips in various scanning probe measurements. Conversely, we have learned much about nanotube structures and properties from STM, STS, and scanning gate measurements.

The electrical properties of nanotubes are dominated by the graphitic π electrons, and many of the electronic phenomena can be explained by simple, nearly analytical models that consider only the two uppermost bands of graphite. However, complex electron-correlation effects emerge at low temperatures, which are best described in a many-body Luttinger liquid picture. Mechanical deformations, defects or highly resistive contacts isolate nanotube electrons and lead to very small quantum dots, in which Coulomb blockade effects can be observed at relatively high temperatures. This has enabled the formation of single-electron transistors

at room temperature. Even with current relatively crude nanoscale manipulation techniques, ingenious processing steps have led to nanotube-based experimental circuitry for both memory and logic operations.

Although this review focused on mechanical and electrical properties, there is also significant interest in other areas, including field emission, battery applications, hydrogen storage, optical limiting, and others. Furthermore, carbon nanotubes are at this time the most prevalent but hardly unique nanotubular structures. Apart from the well-known BN and mixed C-B-N nanotubes, MoS_2 and WS_2 nanotubes have been made, as well as more exotic structures.

Because of their well-defined structure and relative simplicity, nanotubes serve as a convenient test bed for many of the concepts of nanoscale physics and materials science. Many of the issues first addressed with nanotubes will likely be revisited with other nanoscale and molecular systems, including biomolecular ones.

It is difficult to speculate on what the ultimate commercial applications of nanotubes will be, but some are likely to appear in the near future. In particular, nanotube-based electron emitters in flat panel displays seem to be at an advanced stage of development, and relatively little material is required to produce them.

The extraordinary promise and the many challenges of emerging nanotube technology have attracted many workers to this field, which continues to grow quickly. The recent breakthroughs have also generated a substantial amount of excitement, and the expectations for rapid progress remain high. We can look forward to hearing more about this important class of materials in the near future.

The *Annual Review of Materials Research* is online at http://matsci.annualreviews.org

LITERATURE CITED

1. Iijima S. 1991. *Nature* 354:56
2. Dresselhaus MS, Dresselhaus G, Eklund PC. 1996. *Science of Fullerenes and Carbon Nanotubes*. San Diego: Academic
3. Ebbesen TW, ed. 1997. *Carbon Nanotubes: Preparation and Properties*. Boca Raton, FL: CRC Press
4. Dresselhaus MS, Avouris P, eds. 2001. *Carbon Nanotubes*. Berlin: Springer Verlag
5. Maiti A, Brabec CJ, Roland C, Bernholc J. 1995. *Phys. Rev. B* 52:14850
6. Tans SJ, Devoret MH, Dai HJ, Thess A, Smalley RE, et al. 1997. *Nature* 386:474
7. Bockrath M, Cobden DH, McEuen PL, Chopra NG, Zettl A, et al. 1997. *Science* 275:1922
8. Iijima S, Brabec C, Maiti A, Bernholc J. 1996. *J. Chem. Phys.* 104:2089
9. Brenner DW. 1989. In *Atomic Scale Calculations in Materials Science*, ed. J Tersoff, D Vanderbilt, V Vitek, Symp. Proc. No. 141:59. Pittsburgh: Mater. Res. Soc.
10. Brenner DW. 1991. *Phys. Rev. B* 42:9458
11. Falvo MR, Clary GJ, Taylor RM, Chi V, Brooks FP, et al. 1997. *Nature* 389:582
12. Yakobson BI, Brabec CJ, Bernholc J. 1996. *Phys. Rev. Lett.* 76:2511
13. Tombler TW, Zhou CW, Alexseyev L, Kong J, Dai HJ, et al. 2000. *Nature* 405:769
14. Maiti A. 2000. *Chem. Phys. Lett.* 331:21
15. Srivastava D, Menon M, Cho KJ. 1999. *Phys. Rev. Lett.* 83:2973

16. Mazzoni MSC, Chacham H. 2000. *Appl. Phys. Lett.* 76:1561
17. Briggs E, Sullivan D, Bernholc J. 1995. *Phys. Rev. B* 52:5471
18. Briggs E, Sullivan D, Bernholc J. 1996. *Phys. Rev. B* 54:14362
19. Buongiorno Nardelli M, Yakobson BI, Bernholc J. 1998. *Phys. Rev. B* 57:R4277
20. Stone AJ, Wales DJ. 1986. *Chem. Phys. Lett.* 128:501
21. Yakobson BI. 1998. *Appl. Phys. Lett.* 72: 918
22. Buongiorno Nardelli M, Yakobson BI, Bernholc J. 1998. *Phys. Rev. Lett.* 81: 4656
23. Orlikowski D, Buongiorno Nardelli M, Bernholc J, Roland C. 1999. *Phys. Rev. Lett.* 83:4132
24. Zhao Q, Buongiorno Nardelli M, Bernholc J. 2002. *Phys. Rev. B.* In press
25. Zhang PH, Lammert PE, Crespi VH. 1998. *Phys. Rev. Lett.* 81:5346
26. Walters DA, Ericson LM, Casavant MJ, Liu J, Colbert DT, et al. 1999. *Appl. Phys. Lett.* 74:3803
27. Yu MF, Files BS, Arepalli S, Ruoff RS. 2000. *Phys. Rev. Lett.* 84:5552
28. Robertson DH, Mintmire JW, Brenner DW. 1992. *Phys. Rev. B* 45:12592
29. Krishnan A, Dujardin E, Ebbesen TW, Yianilos PN, Treacy MMJ. 1998. *Phys. Rev. B* 58:14013
30. Srivastava D, Brenner DW, Schall JD, Ausman KD, Yu MF, Ruoff RS. 1999. *J. Phys. Chem. B* 103:4330
31. Ajayan P, Schadler L, Giannaris C, Rubio A. 2000. *Adv. Mater.* 12:750
32. Qian D, Dickey EC, Andrews R, Rantell T. 2000. *Appl. Phys. Lett.* 76:2868
33. Bower C, Rosen R, Jin L, Han J, Zhou O. 1999. *Appl. Phys. Lett.* 74:3317
34. Andrews R, Jacques D, Rao AM, Rantell T, Derbyshire F, et al. 1999. *Appl. Phys. Lett.* 75:1329
35. Wood JR, Zhao Q, Frogley MD, Meurs ER, Prins AD, et al. 2000. *Phys. Rev. B* 62:7571
36. Hadjiev VG, Iliev MN, Arepalli S, Nikolaev P, Files BS. 2001. *Appl. Phys. Lett.* 78:3193
37. Zhao Q, Wood JR, Wagner HD. 2001. *Appl. Phys. Lett.* 78:1748
38. Lordi V, Yao N. 2000. *J. Mater. Res.* 15: 2770
39. Frankland S, Brenner D. 1999. *Mat. Res. Soc. Symp. Proc.* 593:199
40. Frankland SJ, Caglar A, Brenner DW, Griebel M. 2002. *Phys. Chem.* In press
41. Hamada N, Sawada S, Oshiyama A. 1992. *Phys. Rev. Lett.* 68:1579
42. Blase X, Benedict LX, Shirley EL, Louie SG. 1994. *Phys. Rev. Lett.* 72:1878
43. Delaney P, Choi HJ, Ihm J, Louie SG, Cohen ML. 1998. *Nature* 391:466
44. Kwon YK, Tomanek D. 1998. *Phys. Rev. B* 58:R16001
45. Balents L, Fisher MPA. 1997. *Phys. Rev. B* 55:11973
46. Egger R, Gogolin AO. 1997. *Phys. Rev. Lett.* 79:5082
47. Kane C, Balents L, Fisher MPA. 1997. *Phys. Rev. Lett.* 79:5086
48. Krotov YA, Lee DH, Louie SG. 1997. *Phys. Rev. Lett.* 78:4245
49. Tans SJ, Devoret MH, Groeneveld RJA, Dekker C. 1998. *Nature* 394:761
50. Bockrath M, Cobden DH, Lu J, Rinzler AG, Smalley RE, et al. 1999. *Nature* 397:598
51. Heyd R, Charlier A, McRae E. 1997. *Phys. Rev. B* 55:6820
52. Yang L, Han J. 2000. *Phys. Rev. Lett.* 85:154
53. Lambin P, Meunier V, Henrard L, Lucas AA. 2000. *Carbon* 38:1713
54. Gallagher M, Chen D, Jacobsen B, Sarid D, Lamb L, et al. 1993. *Surf. Sci. Lett.* 281:335
55. Zhang Z, Lieber CM. 1993. *Appl. Phys. Lett.* 62:2792
56. Ge M, Sattler K. 1993. *Science* 260:515
57. Lin N, Ding J, Yang S, Cue N. 1996. *Carbon* 34:1295
58. Ge MH, Sattler K. 1994. *Appl. Phys. Lett.* 65:2284
59. Wildoer JWG, Venema LC, Rinzler AG,

Smalley RE, Dekker C. 1998. *Nature* 391: 59
60. Odom TW, Huang JL, Kim P, Lieber CM. 1998. *Nature* 391:62
61. Maruyama Y, Takase T, Yoshida M, Kogure K, Suzuki K. 1999. *Fullerene Sci. Technol.* 7:211
62. Hassanien A, Tokumoto M, Kumazawa Y, Kataura H, Maniwa Y, et al. 1998. *Appl. Phys. Lett.* 73:3839
63. Krasheninnikov AV, Nordlund K, Sirvio M, Salonen E, Keinonen J. 2001. *Phys. Rev. B* 63:5405
64. Ouyang M, Huang JL, Cheung CL, Lieber CM. 2001. *Science* 291:97
65. Clauss W, Bergeron DJ, Johnson AT. 1998. *Phys. Rev. B* 58:R4266
66. Meunier V, Lambin P. 1998. *Phys. Rev. Lett.* 81:5588
67. Venema LC, Meunier V, Lambin P, Dekker C. 2000. *Phys. Rev. B* 61:2991
68. Clauss W, Bergeron D, Freitag M, Kane C, Mele E, Johnson A. 1999. *Europhys. Lett.* 47:601
69. Kane CL, Mele EJ. 1999. *Phys. Rev. B* 59: R12759
70. Mark GI, Biro LP, Gyulai J. 1998. *Phys. Rev. B* 58:12645
71. Mark GI, Biro LP, Gyulai J, Thiry PA, Lucas AA, Lambin P. 2000. *Phys. Rev. B* 62:2797
72. Rubio A, Sanchez-Portal D, Artacho E, Ordejon P, Soler JM. 1999. *Phys. Rev. Lett.* 82:3520
73. Rubio A. 1999. *Appl. Phys. A* 68:275
74. Tsukada M, Shima N. 1987. *J. Phys. Soc. Jpn.* 56:2875
75. Meunier V, Senet P, Lambin P. 1999. *Phys. Rev. B* 60:7792
76. Tersoff J, Hamann DR. 1983. *Phys. Rev. Lett.* 50:1998
77. Meunier V, Lambin P. 2000. *Carbon* 38: 1729
78. Orlikowski D, Buongiorno Nardelli M, Bernholc J, Roland C. 2000. *Phys. Rev. B* 61:14194
79. Lambin P, Meunier V, Rubio A. 2000. *Phys. Rev. B* 62:5129
80. Ouyang M, Huang JL, Cheung CL, Lieber CM. 2001. *Science* 292:702
81. Kim P, Odom TW, Huang JL, Lieber CM. 2000. *Carbon* 38:1741
82. Wirth I, Eisebitt S, Kann G, Eberhardt W. 2000. *Phys. Rev. B* 61:5719
83. Charlier JC, Lambin P. 1998. *Phys. Rev. B* 57:R15037
84. White CT, Mintmire JW. 1998. *Nature* 394:29
85. Carroll DL, Redlich P, Ajayan PM, Charlier JC, Blase X, et al. 1997. *Phys. Rev. Lett.* 78:2811
86. Kim P, Odom TW, Huang JL, Lieber CM. 1999. *Phys. Rev. Lett.* 82:1225
87. Venema LC, Wildoer JWG, Janssen JW, Tans SJ, Tuinstra HLJT, et al. 1999. *Science* 283:52
88. Beenakker C, van Houten H. 1991. *Solid State Phys.* 44:1
89. Landauer R. 1970. *Philos. Mag.* 21: 863
90. Datta S. 1995. *Electronic Transport in Mesoscopic Systems*. Cambridge, UK: Cambridge Univ. Press
91. Ferry DK, Goodnick SM. 1997. *Transport in Nanostructures*. Cambridge, UK: Cambridge Univ. Press
92. Tian W, Datta S. 1994. *Phys. Rev. B* 49: 5097
93. Saito R, Dresselhaus G, Dresselhaus MS. 1996. *Phys. Rev. B* 53:2044
94. Chico L, Benedict LX, Louie SG, Cohen ML. 1996. *Phys. Rev. B* 54:2600
95. Tamura R, Tsukada M. 1997. *Phys. Rev. B* 55:4991
96. Tamura R, Tsukada M. 1998. *Phys. Rev. B* 58:8120
97. Anantram MP, Govindan TR. 1998. *Phys. Rev. B* 58:4882
98. Choi HJ, Ihm J. 1999. *Phys. Rev. B* 59: 2267
99. Kong K, Han S, Ihm J. 1999. *Phys. Rev. B* 60:6074
100. Buongiorno Nardelli M. 1999. *Phys. Rev. B* 60:7828
101. Buongiorno Nardelli M, Bernholc J. 1999. *Phys. Rev. B* 60:R16338

102. Sanvito S, Kwon YK, Tomanek D, Lambert CJ. 2000. *Phys. Rev. Lett.* 84:1974
103. Yoon YG, Mazzoni MSC, Choi HJ, Ihm J, Louie SG. 2001. *Phys. Rev. Lett.* 86:688
104. Larade B, Taylor J, Mehrez H, Guo H. 2001. *Phys. Rev. B* 6407:5420
105. Buongiorno Nardelli M, Fattebert JL, Bernholc J. 2001. *Phys. Rev. B* 64: 245423
106. Lopez-Sancho M, Lopez-Sancho J, Rubio J. 1984. *J. Phys. F: Metal Phys.* 14:1205
107. Lopez-Sancho M, Lopez-Sancho J, Rubio J. 1985. *J. Phys. F: Metal Phys.* 15:851
108. Fisher D, Lee P. 1981. *Phys. Rev. B* 23: 6851
109. Meir Y, Wingreen N. 1992. *Phys. Rev. Lett.* 68:2512
110. Chico L, Crespi VH, Benedict LX, Louie SG, Cohen ML. 1996. *Phys. Rev. Lett.* 76: 971
111. White CT, Todorov TN. 1998. *Nature* 393: 240
112. McEuen PL, Bockrath M, Cobden DH, Yoon YG, Louie SG. 1999. *Phys. Rev. Lett.* 83:5098
113. Frank S, Poncharal P, Wang ZL, de Heer WA. 1998. *Science* 280:1744
114. Choi HJ, Ihm J, Yoon YG, Louie SG. 1999. *Phys. Rev. B* 60:R14009
115. Delaney P, Ventra MD, Pantelides ST. 1999. *Appl. Phys. Lett.* 75:3787
116. Liang WJ, Bockrath M, Bozovic D, Hafner JH, Tinkham M, Park H. 2001. *Nature* 411:665
117. Kong J, Yenilmez E, Tombler TW, Kim W, Dai HJ, et al. 2001. *Phys. Rev. Lett.* 87: 106801
118. Choi HJ, Ihm J, Louie SG, Cohen ML. 2000. *Phys. Rev. Lett.* 84:2917
119. Bockrath M, Liang WJ, Bozovic D, Hafner JH, Lieber CM, et al. 2001. *Science* 291:283
120. Collins PG, Bradley K, Ishigami M, Zettl A. 2000. *Science* 287:1801
121. Jhi SH, Louie SG, Cohen ML. 2000. *Phys. Rev. Lett.* 85:1710
122. Kong J, Franklin NR, Zhou CW, Chapline MG, Peng S, et al. 2000. *Science* 287:622
123. Bezryadin A, Verschueren ARM, Tans SJ, Dekker C. 1998. *Phys. Rev. Lett.* 80:4036
124. Paulson S, Falvo MR, Snider N, Helser A, Hudson T, et al. 1999. *Appl. Phys. Lett.* 75: 2936
125. Rochefort A, Avouris P, Lesage F, Salahub DR. 1999. *Phys. Rev. B* 60:13824
126. Orlikowski D, Mehrez H, Taylor J, Guo H, Wang J, Roland C. 2001. *Phys. Rev. B* 6315:5412
127. Mazzoni MSC, Chacham H. 2000. *Phys. Rev. B* 61:7312
128. Bozovic D, Bockrath M, Hafner JH, Lieber CM, Park H, Tinkham M. 2001. *Appl. Phys. Lett.* 78:3693
129. Postma HWC, Teepen T, Yao Z, Grifoni M, Dekker C. 2001. *Science* 293:76
130. Kilic C, Ciraci S, Gulseren O, Yildirim T. 2000. *Phys. Rev. B* 62:R16345
131. Tans SJ, Verschueren ARM, Dekker C. 1998. *Nature* 393:49
132. Martel R, Schmidt T, Shea HR, Hertel T, Avouris P. 1998. *Appl. Phys. Lett.* 73:2447
133. Bachtold A, Henny M, Tarrier C, Strunk C, Schonenberger C, et al. 1998. *Appl. Phys. Lett.* 73:274
134. Xue YQ, Datta S. 1999. *Phys. Rev. Lett.* 83:4844
135. Brandbyge M, Sorensen M, Jacobsen K. 1997. *Phys. Rev. B* 56:14956
136. Anantram MP, Datta S, Xue YQ. 2000. *Phys. Rev. B* 61:14219
137. Cobden DH, Bockrath M, McEuen PL, Rinzler AG, Smalley RE. 1998. *Phys. Rev. Lett.* 81:681
138. Mehrez H, Guo H, Wang J, Roland C. 2001. *Phys. Rev. B* 63:245410
139. Meir Y, Wingreen N, Lee P. 1991. *Phys. Rev. Lett.* 66:3048
140. Beenakker C. 1991. *Phys. Rev. B* 44:1646
141. Tsukagoshi K, Alphenaar BW, Ago H. 1999. *Nature* 401:572
142. Mehrez H, Taylor J, Guo H, Wang J, Roland C. 2000. *Phys. Rev. Lett.* 84: 2682
143. Morpurgo AF, Kong J, Marcus CM, Dai H. 1999. *Science* 286:263
144. Wei YD, Wang J, Guo H, Mehrez H,

Roland C. 2001. *Phys. Rev. B* 6319: 195412
145. Andreev A. 1964. *Sov. Phys. JEPT* 19: 1228
146. Roland C, Buongiorno Nardelli M, Wang J, Guo H. 2000. *Phys. Rev. Lett.* 84:2921
147. Yao Z, Postma HWC, Balents L, Dekker C. 1999. *Nature* 402:273
148. Fuhrer MS, Nygard J, Shih L, Forero M, Yoon YG, et al. 2000. *Science* 288:494
149. Rueckes T, Kim K, Joselevich E, Tseng GY, Cheung CL, Lieber CM. 2000. *Science* 289:94
150. Paulson S, Helser A, Buongiorno Nardelli M, Taylor RM, Falvo M, et al. 2000. *Science* 290:1742
151. Buldum A, Lu JP. 2001. *Phys. Rev. B* 6316:1403
152. Loenard F, Tersoff J. 2000. *Phys. Rev. Lett.* 85:4767
153. Satishkumar BC, Thomas PJ, Govindaraj A, Rao CNR. 2000. *Appl. Phys. Lett.* 77: 2530
154. Papadopoulos C, Raktin A, Li J, Vedeneev AS, Xu JM. 2000. *Phys. Rev. Lett.* 85:3476
155. Treboux G, Lapstun P, Silverbrook K. 1999. *Chem Phys. Lett.* 306:402
156. Andriotis AN, Menon M, Srivastava D, Chernozatonskii L. 2001. *Phys. Rev. Lett.* 87:6802
157. Baughman RH, Cui CX, Zakhidov AA, Iqbal Z, Barisci JN, et al. 1999. *Science* 284:1340
158. Collins PC, Arnold MS, Avouris P. 2001. *Science* 292:706
159. Bachtold A, Hadley P, Nakanishi T, Dekker C. 2001. *Science* 294:1317
160. Derycke V, Martel R, Appenzeller J, Avouris P. 2001. *Nanoletter* 1:453

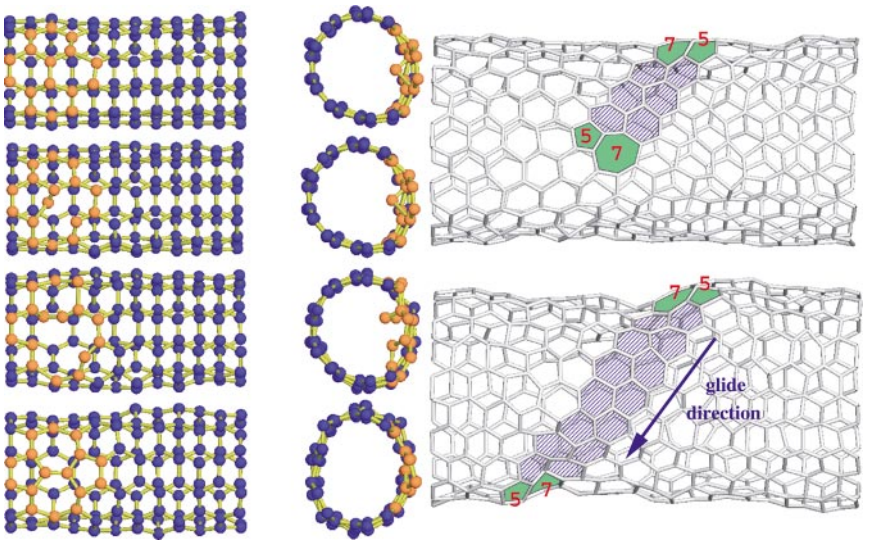

Figure 3 (*Left panel*) Quantum molecular dynamics simulations show that nanotubes initiate breakage by a bond rotation, where a pair of atoms rotates about the center of their bond and converts four hexagons (highlighted in *red*) into a 5-7-7-5 defect. The barrier for this rotation is very high, which further increases the exceptional strength of nanotubes. See text. (*Right panel*) The separation and glide of 5-7 defects in a molecular dynamics simulation at high temperature. This glide constitutes a plastic deformation. Adapted from Reference (19).

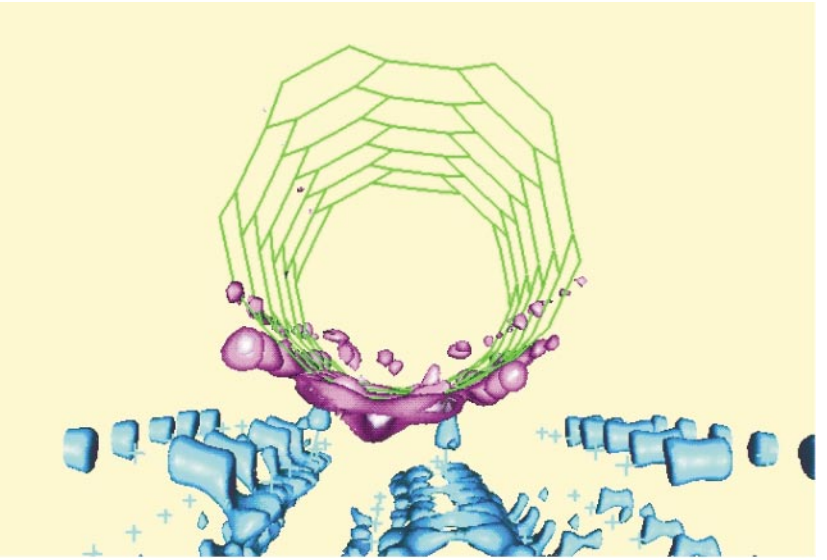

Figure 9 Charge difference plot for the nanotube-Al contact. *Purple* areas indicate electron depletion, *blue* areas indicate electron accretion.